Chemical diffusion of fluorine in phlogopite

Kai Zhang, Hanyong Liu, Jannick Ingrin, Baohua Zhang, Xiaozhi Yang

Journal Pre-proofs

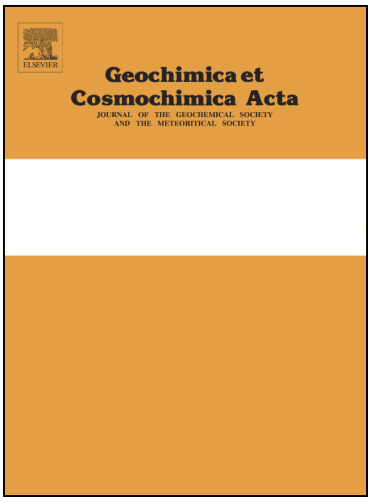

Chemical diffusion of fluorine in phlogopite

Kai Zhang, Hanyong Liu, Jannick Ingrin, Baohua Zhang, Xiaozhi Yang

PII: S0016-7037(22)00327-1
DOI: https://doi.org/10.1016/j.gca.2022.06.039
Reference: GCA 12703

To appear in: *Geochimica et Cosmochimica Acta*

Received Date: 13 December 2021
Revised Date: 28 June 2022
Accepted Date: 29 June 2022

Please cite this article as: Zhang, K., Liu, H., Ingrin, J., Zhang, B., Yang, X., Chemical diffusion of fluorine in phlogopite, *Geochimica et Cosmochimica Acta* (2022), doi: https://doi.org/10.1016/j.gca.2022.06.039

Chemical diffusion of fluorine in phlogopite

Kai Zhang[a], Hanyong Liu[a], Jannick Ingrin[b], Baohua Zhang[c], Xiaozhi Yang[a, d] *

[a] State Key Laboratory for Mineral Deposits Research, School of Earth Sciences and Engineering, Nanjing University, Nanjing 210023, China

[b] Univ. Lille, CNRS, INRAE, Central Lille, UMR 8207, UMET - Unité Matériaux et Transformations, F-59000 Lille, France

[c] Key Laboratory of Geoscience Big Data and Deep Resource of Zhejiang Province, School of Earth Sciences, Zhejiang University, Hangzhou 310027, China

[d] Frontiers Science Center for Critical Earth Material Cycling, Nanjing University, Nanjing 210023, China

* corresponding author (xzyang@nju.edu.cn)

Abstract

Fluorine is a minor yet important component of volatiles in silicate minerals, and affects greatly the physicochemical properties of the host materials. The diffusivity of fluorine provides critical information for quantitatively understanding its many effects, but very few studies have been documented. Here we evaluated the orientation-related chemical diffusion of fluorine in phlogopite, by conducting experiments on single crystal samples. Runs were carried out by the diffusion couple technique at 1 GPa and 700-800 ºC, and durations were typically 25-264 hours. Concentration profiles of fluorine in recovered samples and chemical compositions of minerals were analyzed by electron microprobe, and sample water content was determined by Fourier-transform infrared spectroscopy. The results show that, under the experimental conditions, the fluorine diffusivity is on

the order of 10^{-19} to 10^{-17} m^2/s and is slightly anisotropic. The diffusion is fast along the direction ⊥(110) and slow along the direction ⊥(001), with the direction ⊥(010) falling between them, and the activation energy is 176 to 246 kJ/mol along the three directions. The comparison of the diffusivity data of fluorine with those reported for other species in phlogopite and fluorine in other minerals suggests a strong enhancement of the ionic diffusion along the interlayer direction, thus the diffusivity anisotropy, by the presence of molecular H_2O in the system. The theoretically calculated electrical conductivity of phlogopite, by applying the Nernst-Einstein relation and our determined diffusion data, is remarkably lower than that experimentally measured for the phlogopite with the same fluorine content and with conduction dominated by fluorine. This indicates that the self diffusion of fluorine in phlogopite is much faster than its chemical diffusion, and/or that the mobility of fluorine is largely different between the diffusion and the conductivity experiments. The diffusivity data provide crucial constraints on the closure temperature of fluorine in phlogopite, which is critical for the kinetic analyses of preserved fluorine zonation in natural phlogopites.

Keywords:

Fluorine; diffusion; phlogopite; experimental studies

1. Introduction

Fluorine, the most abundant halogen element, is a minor yet important component in Earth's interior. The concentration is up to several weight percent of fluorine in melts (Aiuppa et al., 2009), and the volume proportion can be significant in volcano-released gases (Symonds et al., 1994). Traditionally, the main host of fluorine is often attributed

to some hydrous fluorine-bearing minerals, e.g., micas, amphibole and apatite (Smith, 1981; Edgar and Charbonneau, 1991; Newsom, 1995; Aiuppa et al., 2009). As the most electronegative and the most chemically active nonmetallic element, fluorine plays an important role in determining many physicochemical properties of the host minerals. In particular, fluorine affects greatly the phase stability (Foley et al., 1986), incorporation of structural water/hydroxyl (Robert et al., 1993), electrical conductivity (Li et al., 2016, 2017), partitioning of trace elements relative to melts (Li and Hermann, 2017), and thermodynamic behaviors and hydrogen bonding (Liu et al., 2021a). Understanding the diffusion of fluorine in minerals is key for quantitatively assessing its many properties. Unfortunately, our knowledge of fluorine diffusion in minerals of geological interest is surprisingly limited.

Phlogopite is one of the most important fluorine-containing minerals. It influences the recycling of fluorine and water (Frost, 2006; Schmidt and Poli, 2014), the melting of mantle rocks (Mysen and Boettcher, 1975; Sudo and Tatsumi, 1990), the formation of potassium-rich metasomatic melts or fluids (Foley, 1993; Condamine and Medard, 2014), and the origin of regional electrical anomalies in the shallow lithosphere (Li et al., 2016, 2017). In this study, we have experimentally examined the orientation-related chemical diffusion of fluorine in phlogopite, by adopting the diffusion couple technique. Two natural phlogopite single crystals with contrasting contents of fluorine were used, and the experiments were carried out at 1 GPa and 700-800 ºC. The obtained diffusivity is on the order of 10^{-19} to 10^{-17} m^2/s, being slightly anisotropic, and the relevant diffusion laws are established. The data offer novel insights into the fluorine-involved

electrical conductivity and diffusivity in phlogopite and the kinetic analyses of fluorine zonation in natural phlogopites.

2. Experiments and methods

2.1 Starting materials

Starting materials were two natural gem-quality phlogopite single crystals (Fig. 1): one is of dark brown color from Afghanistan (Phl-A, with 0.56 wt.% fluorine), and the other is of light yellow color from unknown locality (Phl-B, with 2.71 wt.% fluorine). Because the physicochemical properties of a given mineral at elevated specific pressure and temperature are mainly determined by its chemical composition, the general results of this study are unaffected by the localities of the samples. The two crystals are pseudo-hexagonal and tabular, 10 to 30 mm in size. Both starting crystals are homogeneous in major and minor elements and water (structural OH) contents (Table 1). Except fluorine, the two samples have similar compositions, in particular for the most abundant Si, Al, Mg and K.

The starting phlogopites were cut with a diamond wire saw into blocks of around 2×2×1.5 mm, by considering the three fundamental (001), (010) and (110) planes (Fig. 1). The blocks were then carefully polished with 0.25 μm diamond powder and colloidal silica, for the subsequent experiments on fluorine diffusion perpendicular to these three planes. These three directions are not all coincident with the primary axes (*a*, *b* and *c*) of phlogopite, because it is a monoclinic mineral. In each experimental run, two coupled blocks of the two starting phlogopites, Phl-A and Phl-B with the same orientation, were chosen as the diffusion couples.

2.2 Diffusion experiments

Diffusion experiments were carried out at 1 GPa and 700-800 ºC in an end-loaded piston-cylinder press. The temperature range was chosen by considering run durations (e.g., unrealistically long to produce a measurable diffusion path at lower temperature) and by avoiding devolatilization/breakdown of phlogopite (e.g., at higher temperature). Capsule design is sketched in Fig. 2. Coupled phlogopite blocks were wrapped in a thin Ni foil, and were then packed, along with the fine powder of inert soft hexagonal boron nitride (BN), into a Ni capsule (ID 4.2 mm, OD 5 mm and length 10 mm). The capsule was loaded into a 0.75″ piston-cylinder assembly made of talc, Pyrex glass, graphite (heater) and crushable alumina, and was sealed by mechanical compression in the press. Pressure was calibrated against the quartz-coesite and kyanite-sillimanite transitions, and a fraction correction of 18% was applied. Temperature was controlled by a type-S thermocouple, and fluctuation in each run was usually within ±1 ºC. Run duration was 25-264 hours, depending on experimental temperature (Table 2). Runs with increasing duration (25 vs. 150 hours) at otherwise identical conditions ((001) plane and 800 ºC) were also carried out. At the end of each run, sample was quenched by powering off the heating circuit, and pressure was then slowly released.

Minor green NiO was detected in recovered capsules (Appendix), due probably to the reaction of Ni and residual O_2 in charges (e.g., $2Ni + O_2 = 2NiO$). The redox state was thus buffered by the Ni-NiO pair. Recovered samples in each capsule were cut into two halves along the lengthwise direction, which is perpendicular to the interface of the diffusion couples. One half was for measurements of major and minor elements, as well

as diffusion profiles and elemental mappings, and the other half for analyses of water (OH) content.

2.3 Sample characterization

Chemical compositions, diffusion profiles and elemental mappings were measured using a JEOL JXA-8230 electron microprobe analyzer. Operating conditions were: 15 kV accelerating voltage, 10 nA beam current for chemical compositions and diffusion profiles and 20 nA for elemental mappings, 5 μm beam size for chemical compositions, 1 μm for diffusion profiles and 0.2 μm for elemental mappings, and a counting time of 10 and 5 seconds for the peak and background. Natural minerals and synthetic oxides were used as the standards, and raw data were reduced with the routine atomic number-absorption-fluorescence (ZAF) correction procedure. Profile analyses were performed for both fluorine and the common major and minor elements. Backscatter electron (BSE) imaging was performed with a field emission scanning electron microscope (FESEM, Zeiss Sigma 500).

Water content was determined by Fourier-transform infrared (FTIR) spectroscopy. The general principle can be described by the Beer-Lambert law, $C_w=Abs_{tot}\cdot 1.8/(\rho\cdot\varepsilon)$, where C_w is the water content, Abs_{tot} is the total integrated absorbance (normalized to 1 cm thickness), ρ is the density, and ε is the calibration coefficient. Consequently, C_w is determined by the Abs_{tot}, given an externally calibrated ε. FTIR spectra were collected with a Bruker Vertex 70V spectrometer coupled to a Hyperion 2000 microscope (globar source, KBr-Ge beam splitter, MCT detector and ZnSe wire-grid polarizer). Polarized analyses along three orthogonal directions, following Shuai and Yang (2017), were

used to characterize the water content of the starting phlogopites (Appendix). The recovered samples were small, fractured and easily split into cleavage flakes, making them hard to prepare for polarized measurements. Therefore, unpolarized analyses perpendicular to the (001) plane were performed on the starting and recovered samples for assessing relative changes of water content in the runs (Appendix). Thickness of polished samples was ~5 to 13 μm, as measured with a Mitutoyo digital micrometre. The absorbance was integrated from 3500 to 3800 cm^{-1} with a spline fit method for baseline subtractions, and the uncertainty is 10-15%, as estimated by performing several reasonable baseline corrections to representative spectra. The phlogopite-specific calibration coefficient of Rouxhet (1970), ~7800 L mol^{-1} cm^{-2}, was used to obtain the water content. The adoption of this coefficient does not change the general results of this study.

2.4 Determination of diffusivity

The quantitative analyses of major and minor elements show no diffusion profiles in the experiments (as will be further shown below). Assuming that the net diffusion of fluorine was one-dimensional in the runs, driven mainly by the concentration contrast between the starting phlogopites and being independent of the fluorine concentration, the diffusion profiles were fitted by the following relation (Crank, 1975):

$$C = \frac{C_1 + C_2}{2} + \frac{C_1 - C_2}{2}\,\mathrm{erf}\left(\frac{x}{2\sqrt{Dt}}\right) \qquad (1a)$$

where C is the concentration of fluorine in the recovered sample at a distance x (relative to the crystal-crystal interface of the diffusion couples which defines the 0 position) and time t (e.g., the run duration), C_1 and C_2 are the maximum and minimum concentrations

of fluorine (e.g., the initial contents of Phl-B and Phl-A in this study), respectively, and D is the diffusivity (or diffusion coefficient). The uncertainty of the obtained diffusivity was propagated from the fittings to the measured data.

To determine if the diffusivity is dependent on the fluorine concentration (e.g., the Matano effect), the diffusion profiles of fluorine in the phlogopite samples were also examined using the Boltzmann-Matano analysis (Matano, 1933), by which the Matano interface at the modelled 0 position could be obtained:

$$D(C^*) = -\frac{1}{2t}\left(\frac{dx}{dC}\right)_{C^*} \int_{C_1}^{C^*} x dC \qquad (1b)$$

where $D(C^*)$ is the composition-dependent diffusivity at the concentration C^*.

3. Results

In general, the samples, excluding the narrow diffusion zones close to the interface of the diffusion couples in each run, demonstrate no change in the composition of major and minor elements before and after the experiment (Table 1). The H_2O content is ~1.23 and 1.04 wt.% for Phl-A and Phl-B, respectively, which are consistent with the values ranging from less than 1 wt.% to slightly exceeding 5 wt.% in natural phlogopites (Frost, 2006) [note: natural phlogopites rarely crystallize under fluorine- and water-saturated conditions, so that the ideal configuration of both fluorine and water is hard to acquire]. Although the absolute water contents of the samples in the run products are difficult to determine with polarized FTIR measurements (Section 2.3), the unpolarized analyses perpendicular to the (001) plane of the starting and recovered samples show almost the same OH absorption bands and integral absorbance for Phl-A or Phl-B (Appendix). As such, the sample water contents in regions away from the diffusion-couple interface did

not change during the experiments. A representative BSE image of a recovered sample, including also the elemental mapping of fluorine across the sample interface, is given in Fig. 3. The interface of the diffusion couples, though easily identified, is not perfectly flat after the experiment. This may have been produced by the non-uniform volume (or surface) changes of the samples at elevated run conditions.

The diffusion-driven fluorine concentration gradients across the sample interface are observed in all the experiments, and the diffusion distance varies with temperature, duration and orientation (see Appendix). A representative profile is presented in Fig. 4a, along with the fit curves by Eq. (1a) and (1b). No zoned distribution is detected for the sluggish major and minor elements (Fig. 4b-c). It is likely that the water concentration in each recovered phlogopite varies close to the crystal-crystal interface, in association with the zoned fluorine profile. Unfortunately, this is difficult to verify because of the relatively poor resolution of the FTIR technique, e.g., usually beyond 20×20 μm.

With Eq. (1), the diffusivity of fluorine could be calculated for each of the studied temperatures and orientations (Table 2). The crystal-crystal and the Matano interfaces are well coincident, and the fit curves and the diffusivity by applying Eq. (1a) and (1b) to the data in each run are essentially the same (Fig. 4a and Table 2). Accordingly, the diffusivity is independent of the fluorine concentration. The time-series experiments at otherwise comparable conditions show that the diffusion path is longer in the run with increasing duration, and that the diffusivity is basically the same between the runs with contrasting durations (Appendix and Table 2). For simplicity, the diffusivity obtained

with Eq. (1a) are used for the discussion below. The data are further modelled by the Arrhenius relation:

$$D = D_0 \exp(-\frac{E}{RT}) \quad (2)$$

where D_0 is the pre-exponential factor, E is the activation energy, R is the universal gas constant, and T is the absolute temperature. Eq. (2) is applied to fit the data along each direction, and the fitting parameters are given in Table 2. The activation energy is ~176 to 246 kJ/mol along the studied directions. The diffusivity, and their fits, are projected in Fig. 5. The diffusion along the three directions is quantitatively described by:

$$D_{\perp(001)} = 10^{-5.94 \pm 0.87} \exp(-\frac{246 \pm 16 \text{ kJ/mol}}{RT}) \text{ m}^2/\text{s} \quad (3a)$$

$$D_{\perp(010)} = 10^{-7.87 \pm 0.58} \exp(-\frac{198 \pm 11 \text{ kJ/mol}}{RT}) \text{ m}^2/\text{s} \quad (3b)$$

$$D_{\perp(110)} = 10^{-8.75 \pm 0.22} \exp(-\frac{176 \pm 4 \text{ kJ/mol}}{RT}) \text{ m}^2/\text{s} \quad (3c)$$

The difference in diffusivity between the three directions varies by a factor of about 10 at 700 ºC to 5 at 800 ºC. Therefore, the diffusivity is slightly anisotropic, and regardless of the narrow range of temperature, the results suggest that the degree of the anisotropy is temperature-dependent. Below ~1000 ºC, the diffusion is fast along the direction ⊥(110) and is slow along the direction ⊥(001), with the direction ⊥(010) falling between them. The average bulk diffusivity (D_{GM}) is calculated as the geometric mean (GM) of Eq. (3) by assuming a self-isotopic medium:

$$D_{GM} = \sqrt[3]{D_{\perp(001)} D_{\perp(010)} D_{\perp(110)}} = 10^{-7.42 \pm 0.61} \exp(-\frac{205 \pm 10 \text{ kJ/mol}}{RT}) \text{ m}^2/\text{s} \quad (4)$$

4. Mechanism of fluorine diffusion

Chemical diffusion and self diffusion are two terms frequently used in the studies of diffusion experiments. Chemical diffusion is primarily produced in the presence of

a concentration (or chemical potential) gradient, while self diffusion occurs in systems of homogeneous composition in the absence of chemical potential gradient. Self diffusion is usually assumed to be identical to tracer diffusion, which introduces an isotopic tracer into a material as long as there is no concentration (or chemical potential) gradient. The chemical diffusion of fluorine in phlogopite, as examined in this work, may involve the concurrent transfer of one or several other elements. However, the absence of any zoned diffusion profiles for the major and minor elements, as observed for K and Ti in Fig. 4, suggests that they have played a negligible role, if any, in affecting the fluorine diffusion in our samples.

The storage of fluorine and hydroxyl groups in silicate minerals is highly coupled, by occupying the same sites in the crystal structure and substituting for each other (e.g., Stormer and Carmichael, 1971; Robert et al., 1993; Hazen et al., 1997; Crépisson et al., 2014; Roberge et al., 2015). As such, the diffusion of fluorine in the phlogopite samples was probably dominated by the binary interdiffusion of fluorine and hydroxyl. This has been proposed as the main mechanism for the chemical diffusion of fluorine in biotite (Sallet et al., 2018) and the ionic exchange of fluorine between fluorine-bearing silicate minerals (e.g., apatite and tremolite) and hydrothermal fluids (Brenan, 1994; Brabander et al., 1995). Similar mechanism by the exchange with hydroxyl has also been proposed for the diffusion of other halogens such as chlorine in amphibole (Su et al., 2015). This interpretation fits well with the fact that the diffusivity of fluorine is in fact independent of its concentration in the phlogopites (Section 3). Very likely, when an atom of fluorine moves from one site to another in the lattice, a counter migration of hydroxyl is induced

(but could be complicated as noted below). A diffusion-involved decrease (or increase) of fluorine content in the phlogopite may be accompanied by an increase (or decrease) of hydroxyl content. In this case, the diffusion profiles of hydroxyl across the diffusion-couple interface are expected, but the general pattern should be opposite to that detected for fluorine (Fig. 4a).

Structure refinements have shown that, in phlogopite and other Mg-rich micas, the incorporation of fluorine strongly favors the trioctahedral sites, as a result of the local charge balance around the hydroxyl group (Robert et al., 1993). In trioctahedral sites, the hydroxyl group acts as a point charge, and at best weakly interacts with tetrahedral oxygen, making it easily substituted by fluorine. This is different from the dioctahedral environment where a hydroxyl group interacts via hydrogen bonding with underbonded oxygen of the adjacent tetrahedra, that inhibits the substitution by fluorine. Therefore, the interdiffusion of fluorine and hydroxyl in the phlogopite samples was more likely through their ionic exchange in the trioctahedral sites. The possibility of fluorine (itself) jumping between lattice vacancies, arising from the fact that some hydroxyl sites could be vacant, cannot be ruled out; however, it is at present hard to place further constraints on the extent the diffusion was controlled by this mechanism.

5. Comparison with previous studies

Diffusion experiments have been carried out for several other species in phlogopite, such as argon, oxygen and strontium (Fig. 6a). The previous studies were all conducted on polycrystalline samples, except two cases on single crystal phlogopites for strontium (Hammouda and Cherniak, 2000) and oxygen (Fortier and Giletti, 1991). The chemical

diffusivity of argon in the available reports, broadly comparable though with observable difference (Evernden et al., 1960; Giletti, 1974; Giletti and Tullis, 1977), is similar to or slightly greater than that of fluorine. The comparison is, however, not straightforward, because the movement in the structure differs between the neutral argon and the charged fluorine (and other ions). The comparison with oxygen may be more meaningful, owing to the possible role of hydroxyl in fluorine diffusion (Section 4). The self diffusivity of oxygen (using ^{18}O tracer), as shown in Fortier and Giletti (1991), is highly anisotropic, varying by 3-4 orders of magnitude between the direction //c and $\perp c$ (Fig. 6a). This is in sharp contrast to the 0.5-1 orders of magnitude difference in fluorine diffusivity along three orientations (Fig. 5). The contrast may be linked to: (1) the difference between the chemical and the self diffusivity of oxygen, (2) the chemical effect on diffusivity, (3) the amount of exchangeable sites for diffusion, and (4) the difference in experimental methods. Point (1) is expected to be insignificant by considering the broadly consistent chemical and self diffusivity of oxygen as inferred from the comparable diffusivity of ^{17}O and ^{18}O in feldspar (Freer et al., 1997). Point (2) is not favored because the sample chemistry is similar between Fortier and Giletti (1991) and this study. Point (3) can be a contributing factor, because oxygen has a larger number of exchangeable sites relative to fluorine and perhaps the oxygen diffusivity along the interlayers is facilitated partly by the additional exchangeable sites. Point (4) regarding the study of Fortier and Giletti (1991) at hydrothermal conditions by isotope exchange with a hydrous fluid vs. ours at dry conditions is probably the most important factor for causing the contrast. In addition, the net diffusion of oxygen in Fortier and Giletti (1991)

was in fact not one-dimensional, and the presence of molecular H_2O in the interlayers of their samples may have greatly enhanced the diffusion of oxygen $\perp c$ (thus the anisotropy). For strontium, the chemical diffusivity $//c$ at dry conditions was reported by Hammouda and Cherniak (2000). If the slight anisotropy of fluorine diffusion under dry conditions (Fig. 5) is applicable to other ions, the diffusivity of strontium $\perp c$ might not be significantly different from that of $//c$ as measured by Hammouda and Cherniak (2000).

Concerning fluorine diffusion, the only available data for minerals are those on the chemical diffusion in titanite, a very preliminary result reported in a conference abstract (Berds et al., 2008), and biotite (Sallet et al., 2018). The former experiments were done at dry conditions by exchange with a fluorine-rich apatite, and the latter at hydrothermal conditions by fluorine exchange between tiny biotite grains and a hydrous hydrofluoric (HF) acid, with some grains in the run products analyzed for the fluorine profiles along the interlayers. The fluorine diffusivity in phlogopite is smaller than that in biotite but is greater than that in titanite, both by ~3 to 4 orders of magnitude at a given temperature (Fig. 6b). The difference between phlogopite and biotite could be accounted for by: (1) the different composition of other species such as Si, Ti, Fe and Mg. It has been shown that iron affects lead diffusion in pyroxenes (Cherniak, 1998) and calcium and sodium affect strontium diffusion in feldspars (Cherniak and Watson, 1994). Phlogopite is the Mg endmember of biotite, and it is possible that the fluorine diffusion is influenced by other species; (2) the enhanced diffusivity of biotite by molecular H_2O in the interlayers and the non-one-dimensional diffusion of fluorine in the experiments, as noted above.

In contrast, the difference between phlogopite and titanite may have been accounted for by the different crystal structures and their effects on the fluorine diffusivity. This has been used to explain the different diffusivity of oxygen between different micas (Fortier and Giletti, 1991). In any case, it is interesting to note that the low diffusivity of fluorine in titanite is also associated with experiments performed at dry conditions. The diffusion data of oxygen, strontium and fluorine in phlogopite and fluorine in biotite, phlogopite and titanite indicate that the diffusivity of ionic species is probably much lower at dry than at hydrous conditions.

6. On diffusion and electrical conduction of fluorine

Recent studies have shown that fluorine is an important charge carrier for electrical conduction in fluorine-containing minerals, and that the high electrical conductivity of phlogopite and fluorite could be reasonably attributed to fluorine conduction (Li et al., 2016, 2017; Liu et al., 2019). The conductivity due to the transfer of a charge carrier is linked to its movement, and the Nernst-Einstein relation quantitatively establishes the relationship between the conductivity (σ) and the diffusivity of a charged species:

$$\sigma = \frac{Dc_c q^2}{kT} \tag{5}$$

where c_c is the concentration of the charge carrier, q is the electrical charge of the ion, and k is the Boltzmann constant. The reported activation energy of fluorine conduction in phlogopite is about 134, 179 and 204 kJ/mol along the direction ⊥(110), ⊥(010) and ⊥(001), respectively (Li et al., 2016). In contrast, the activation energy for the chemical diffusion of fluorine in phlogopite is greater, ~176, 198 and 246 kJ/mol along the three directions, respectively (Table 2), although the anisotropy of conductivity by fluorine

conduction is similarly weak as that of diffusivity in diffusion experiments. The smaller activation energy in conductivity than in diffusivity experiments has also been reported for hydrogen (proton) in many minerals, e.g., olivine, pyroxenes, garnet and feldspars (Dai and Karato, 2009; Poe et al., 2010; Yang et al., 2011, 2012; Yang, 2012; Yang and McCammon, 2012; Liu et al., 2019, 2021a, 2021b). By using Eq. (5) and the parameters for the chemical diffusivity of fluorine (Table 2) and by assuming fluorine conduction, we calculated the conductivity of phlogopite with a fluorine content of 2.75 wt.% (Fig. 7). The conductivity is about 7 to 8 orders of magnitude smaller than that experimentally measured by Li et al. (2016) for the phlogopite with the same fluorine content.

The largest assumptions required by Eq. (5) are: (1) the conductivity is dominated by the main charged species, and (2) the mechanism for the movement of the species in conductivity experiments is the same as that in diffusion runs. In theory, the self rather than the chemical diffusivity should be adopted in Eq. (5). The conductivity analyses of Li et al. (2017) on the gem-quality phlogopites with a series of fluorine contents have demonstrated that, under otherwise comparable conditions, the conductivity increases systematically with increasing fluorine content. Accordingly, fluorine is expected to be the main charge carrier in the conductivity experiments. The strong difference between the measured and the calculated conductivity of phlogopite (Fig. 7) would imply that the self diffusion of fluorine is much faster than its chemical diffusion. Possibly, the self diffusivity is ~7-8 orders of magnitude greater than the chemical diffusivity, and is only slightly anisotropic. The chemical diffusion of fluorine in phlogopite, dominated

by the interdiffusion exchange (Section 5), is rate-limited by the self diffusion of fluorine and hydroxyl. An immediate conclusion is that the net diffusivity of hydroxyl in the crystal structure is probably much slower than that of fluorine. This provides an additional but attractive explanation to the above noted strong anisotropy of oxygen self diffusion in phlogopite under hydrous conditions (Fortier and Giletti, 1991). The strongly enhanced diffusivity along the interlayers is related to the fast movement of molecular H_2O (the ^{18}O carrier, see Section 5); however, molecular H_2O is hard to get through the mineral structure, resulting in the transfer of ^{18}O by hydroxyl diffusion and the slow diffusivity perpendicular to the interlayers.

Alternatively, this could reflect the difference between diffusion and conductivity experiments. In diffusion runs, there is a net transfer of the species for both the chemical diffusion in the presence of a (chemical) concentration gradient and the self diffusion in the presence of an isotopic content gradient. In conductivity runs with the alternating voltage impedance spectroscopy which is necessary for characterizing the conductivity of Earth materials (Barsoukov and Macdonald, 2005), both the preparation of samples and the movement of species are different. In the conductivity experiments of Li et al. (2016, 2017), the phlogopite sample in each run is chemically homogeneous, without any chemical or isotopic gradient. Furthermore, the charge carrier oscillates around an equilibrium position, without net displacement (what moves is the electric and magnetic fields, or voltage). Therefore, the mobility of a charge carrier in conductivity runs is not necessarily the same as that of the corresponding species in diffusion experiments. In fact, it has already been reported in material sciences that, even for self diffusivity, the

conductivity calculated with Eq. (5) can be different from that measured for conduction controlled by the same charged species in even the same sample (Borucka et al., 1957; Keller et al., 1979; Andrade, 1993; Marcolongo and Marzari, 2017; France-Lanord and Grossman, 2019). However, all other isotopes of fluorine are extremely short-lived, and it is hard, if not impossible, to test this possibility by experimentally measuring the self diffusivity of fluorine in phlogopite (or other materials).

7. Implications for fluorine exchange analysis in natural samples

In addition to the above aspects on the chemical diffusion of fluorine in phlogopite and its potential impacts for electrical conductivity, the measured data can also be used to evaluate the kinetics of fluorine exchange in natural phlogopite, regarding the closure temperature and the preservation of fluorine zonation.

The closure temperature is a concept for describing a diffusive species in a system undergoing cooling (Dodson, 1973). It is a bulk average temperature recorded between a mineral and an assumed infinite reservoir, and is regarded as an intrinsic characteristic of the mineral, independent of the behavior and properties of other species. Below that temperature, the diffusion rate of the species is insignificant. The closure temperature of fluorine is estimated by the equations below:

$$\frac{E}{RT_{\mathrm{c}}} = \ln\left(-\frac{ART_{\mathrm{c}}^2 D_0}{a^2 E\,\mathrm{d}T/\mathrm{d}t}\right) \tag{6a}$$

$$\frac{E}{RT_{\mathrm{c}}} = \ln\left(-\frac{A'RT_{\mathrm{c}}^2 D_0}{a^2 E\,\mathrm{d}T/\mathrm{d}t}\right) \tag{6b}$$

where T_{c}.is the closure temperature, a is the effective grain dimension (e.g., radius of a spherical grain), and $\mathrm{d}T/\mathrm{d}t$ is the cooling rate. Eq. (6a) is the classic equation by Dodson

(1973), and Eq. (6b) is the modified form by Ganguly and Tirone (1999). The difference between these two equations is the geometric factor A in Eq. (6a), a constant dependent on grain geometry (G, $A = e^G$, e.g., the value of A is ~55 for spherical grains), and A' in Eq. (6b), a parameter related to grain geometry, cooling rate and diffusivity at T_0 (the peak temperature at the onset of or during the cooling, $A' = A \cdot e^g$, where g is a correction term defined by Ganguly and Tirone (1999) and its value is available from their original Fig. 2). Eq. (6b) extends Eq. (6a) to include cases even with arbitrarily small amounts of diffusion, while accounting for the dependence of T_c on T_0.

The calculated results are shown in Fig. 8, as a function of grain radius and cooling rate. The estimated T_c by Eq. (6a) increases with increasing cooling rate and grain radius (Fig. 8a). The modelled T_c of fluorine in biotite, on the basis of the diffusivity data ($\perp c$) of Sallet et al. (2018), is also plotted in Fig. 8a for comparison. The T_c of biotite is lower than that of phlogopite at a given cooling rate. In case of a relatively large grain radius, the closure temperatures yielded by Eq. (6b) commonly deviate from those by Eq. (6a), and the relative deviation becomes smaller with increasing T_0 or decreasing dT/dt (e.g., Ganguly and Tirone, 1999). An example figure of the calculated closure temperature of GM with Eq. (6b) is given in Fig. 8b, plotted as a function of the peak temperature and grain radius at an assumed cooling rate of 1 ºC per million years (Myr). The calculated closure temperatures with Eq. (6a) and (6b) are consistent at small grain sizes, but differ at large grain sizes, with the relative difference being smaller as grain radius decreases and/or peak temperature increases. The observed data trends agree with available work on the closure temperature of other species, e.g., Pb in monazite (Cherniak et al., 2004),

rare earth elements (REE) in enstatite (Cherniak and Liang, 2007), and Fe-Mg in garnet (Zhang et al., 2019) and clinopyroxene (Müller et al., 2013).

These data are used to constrain the fluorine zonation in natural phlogopites. Many studies have documented the zoned distribution of fluorine in phlogopites derived from the crust and mantle (Rimsaite, 1970; Belkin et al., 1988; Krasnova, 2001; Lee et al., 2003; Downes et al., 2006; Giuliani et al., 2016; Kargin et al., 2019). The zoned patterns are usually on the scale of several hundreds of μm to a few mm, e.g., perpendicular to the interlayers (Belkin et al., 1988). The origin of the zoned fluorine could be multiple, e.g., by metasomatism-related secondary fluid modifications or by crystallization under hydrothermal conditions (or both). However, the preservation of the fluorine zonation suggests that the diffusion-driven homogenization of fluorine was insignificant. In light of the diffusion data and closure temperature of fluorine, the kinetics involved with the zonation are analyzed for two possible scenarios of fluid mobility. First, if fluid escaped after the formation of the zonation, which is highly likely owing to the low density and high buoyancy, the behavior of fluorine diffusion was similar to that in our experiments; second, if fluid was still present after the crystal growth, the diffusivity of fluorine might be enhanced, but the enhancement was weak perpendicular to the interlayers (Sections 5 and 6). In either case, our diffusivity data can be reasonably applied, and the GM data are meaningful for the modeling. The cooling rate of phlogopite-bearing samples (e.g., xenoliths) or complex has not been well established, but is usually larger than 1 ºC/Myr (Hammouda and Cherniak, 2000; Sallet et al., 2018). The closure temperature obtained at 1 ºC/Myr (Fig. 8b) thus reflects the bottom boundary, and is expected to be at least

300 to 500 ºC for the scale of the fluorine zonation. This indicates that the prevailing temperature in the system should have been mostly less than ~300 ºC. This agrees with the estimated temperature of mainly 100-300 ºC based on other mineral assemblages or fluid inclusions (Rimsaite, 1970; Belkin et al., 1988; Krasnova, 2001; Lee et al., 2003). Our data could offer more informative constraints on the kinetic processes, if the zoned fluorine along specific orientations of natural phlogopites is quantified.

8. Conclusions

The chemical diffusion of fluorine in phlogopite has been for the first time assessed, through ionic diffusion experiments between gem-quality natural phlogopite crystals of contrasting fluorine contents. The runs were performed in a piston-cylinder press, at 1 GPa and 700-800 ºC and with durations of 25 to 264 hours. The diffusion was probably dominated by the interdiffusion of fluorine and hydroxyl in the structure. We show that the measured diffusivity of fluorine is from 10^{-19} to 10^{-17} m^2/s, and is slightly anisotropic. At a given temperature below ~1000 ºC, the diffusion is fast along the direction ⊥(110) and is slow along the direction ⊥(001), with the direction ⊥(010) falling between them. The comparison with available data on the diffusivity of other species in phlogopite and fluorine in other minerals indicates that the presence of water (i.e., molecular H_2O) may enhance strongly ionic diffusion in the interlayers, as well as the anisotropy of diffusion. The chemical diffusivity of fluorine is used to calculate the electrical conductivity of phlogopite, which is, however, significantly smaller than that experimentally measured for the phlogopite with the same fluorine concentration and with conduction controlled mainly by fluorine. The difference suggests that the self

diffusivity of fluorine is much faster than its chemical diffusivity, and/or that the movement of fluorine differs greatly between diffusion and conductivity experiments. The diffusivity data of fluorine are applied to estimate the closure temperature of fluorine in phlogopite, and the preserved zonation of fluorine in natural phlogopites can now be kinetically analyzed regarding the fluorine exchange.

Acknowledgements

We thank Lingmin Zhang for assistance with electron microprobe measurements. Editorial handing by Wim van Westrenen and constructive comments by Jonathan D. Price and an anonymous reviewer helped to improve the manuscript. This study was supported by National Science Foundation of China (41725008), Research Funds for the Frontiers Science Center for Critical Earth Material Cycling and Fundamental Research Funds for the Central Universities to X.Y.

References

Aiuppa A., Baker D. R. and Webster J. D. (2009) Halogens in volcanic systems. *Chem. Geol.* **263**, 1–18.

Andrade C. (1993) Calculation of chloride diffusion coefficients in concrete from ionic migration measurements. *Cem. Concr. Res.* **23**, 724–742.

Barsoukov E. and Macdonald J. R. (2005) *Impedance Spectroscopy Theory, Experiments and Applications*., John Wiley and Sons, Inc.

Belkin H. E., Cavarretta G., De Vivo B. and Tecce F. (1988) Hydrothermal phlogopite and anhydrite from the SH2 Well, Sabatini volcanic district, Latium, Italy; fluid inclusions and mineral chemistry. *Am. Mineral.* **73**, 775–797.

Berds M. L., Price J. D. and Cherniak D. J. (2008) Fluorine Diffusion in Titanite: Preliminary Results from Experiments. In *American Geophysical Union, Fall Meeting* pp. MR33A-1840.

Borucka A. Z., Bockris J. O. and Kitchener J. A. (1957) Self-diffusion in molten sodium chloride: a test of the applicability of the Nernst—Einstein equation. *Proc. R. Soc. Lond. Ser. Math. Phys. Sci.* **241**, 554–567.

Brabander D. J., Hervig R. L. and Jenkins D. M. (1995) Experimental determination of F-OH interdiffusion in tremolite and significance to fluorine-zoned amphiboles. *Geochim. Cosmochim. Acta* **59**, 3549–3560.

Brenan J. (1994) Kinetics of fluorine, chlorine and hydroxyl exchange in fluorapatite. *Chem. Geol.*

110, 195–210.

Cherniak D. J. (1998) Pb diffusion in clinopyroxene. *Chem. Geol.* **150**, 105–117.

Cherniak D. J. and Liang Y. (2007) Rare earth element diffusion in natural enstatite. *Geochim. Cosmochim. Acta* **71**, 1324–1340.

Cherniak D. J. and Watson E. B. (1994) A study of strontium diffusion in plagioclase using Rutherford backscattering spectroscopy. *Geochim. Cosmochim. Acta* **58**, 5179–5190.

Cherniak D. J., Watson E. B., Grove M. and Harrison T. M. (2004) Pb diffusion in monazite: a combined RBS/SIMS study. *Geochim. Cosmochim. Acta* **68**, 829–840.

Condamine P. and Medard E. (2014) Experimental melting of phlogopite-bearing mantle at 1 GPa: Implications for potassic magmatism. *Earth Planet. Sci. Lett.* **397**, 80–92.

Crank J. (1975) *The Mathematics of Diffusion*. 2nd Edition., Oxford University Press.

Crépisson C., Blanchard M., Bureau H., Sanloup C., Withers A. C., Khodja H., Surble S., Raepsaet C., Béneut K., Leroy C., Giura P. and Balan E. (2014) Clumped fluoride-hydroxyl defects in forsterite: implications for the upper-mantle. *Earth Planet. Sci. Lett.* **390**, 287–295.

Dai L. and Karato S. I. (2009) Electrical conductivity of pyrope-rich garnet at high temperature and high pressure. *Phys. Earth Planet. Inter.* **176**, 83–88.

Dodson M. H. (1973) Closure temperature in cooling geochronological and petrological systems. *Contrib. Mineral. Petrol.* **40**, 259–274.

Downes P. J., Wartho J.-A. and Griffin B. J. (2006) Magmatic evolution and ascent history of the Aries micaceous kimberlite, Central Kimberley Basin, Western Australia: evidence from zoned phlogopite phenocrysts, and UV laser $^{40}Ar/^{39}Ar$ analysis of phlogopite–biotite. *J. Petrol.* **47**, 1751–1783.

Edgar A. D. and Charbonneau H. E. (1991) Fluorine-bearing phases in lamproites. *Mineral. Petrol.* **44**, 125–149.

Evernden J. F., Curtis G. H., Kistler R. W. and Obradovich J. D. (1960) Argon diffusion in glauconite, microcline, sanidine, leucite and phlogopite. *Am. J. Sci.* **258**, 583–604.

Foley S. F. (1993) An experimental study of olivine lamproite: first results from the diamond stability field. *Geochim. Cosmochim. Acta* **57**, 483–489.

Foley S. F., Taylor W. R. and Green D. H. (1986) The effect of fluorine on phase relationships in the system $KAlSiO_4$-Mg_2 SiO_4-SiO_2 at 28 kbar and the solution mechanism of fluorine in silicate melts. *Contrib. Mineral. Petrol.* **93**, 46–55.

Fortier S. M. and Giletti B. J. (1991) Volume self-diffusion of oxygen in biotite, muscovite, and phlogopite micas. *Geochim. Cosmochim. Acta* **55**, 1319–1330.

France-Lanord A. and Grossman J. C. (2019) Correlations from ion pairing and the Nernst-Einstein equation. *Phys. Rev. Lett.* **122**, 136001.

Freer R., Wright K., Kroll H. and Göttlicher J. (1997) Oxygen diffusion in sanidine feldspar and a critical appraisal of oxygen isotope-mass-effect measurements in non-cubic materials. *Philos. Mag. A* **75**, 485–503.

Frost D. J. (2006) The stability of hydrous mantle phases. *Rev. Mineral. Geochem.* **62**, 243–271.

Ganguly J. and Tirone M. (1999) Diffusion closure temperature and age of a mineral with arbitrary extent of diffusion: theoretical formulation and applications. *Earth Planet. Sci. Lett.* **170**, 131–140.

Giletti B. J. (1974) Studies in diffusion I: argon in phlogopite mica. In *Geochemical transport and kinetics* (ed. A. W. Hofmann). Carnegie Institution of Washington, Washington, DC. pp. 107–

115.

Giletti B. J. and Tullis J. (1977) Studies in diffusion, IV. Pressure dependence of Ar diffusion in phlogopite mica. *Earth Planet. Sci. Lett.* **35**, 180–183.

Giuliani A., Phillips D., Kamenetsky V. S. and Goemann K. (2016) Constraints on kimberlite ascent mechanisms revealed by phlogopite compositions in kimberlites and mantle xenoliths. *Lithos* **240–243**, 190–201.

Hammouda T. and Cherniak D. J. (2000) Diffusion of Sr in fluorphlogopite determined by Rutherford backscattering spectrometry. *Earth Planet. Sci. Lett.* **178**, 339–349.

Hazen M., Yang H., Prewitt C. T. and Gasparik T. (1997) Crystal chemistry of superfluorous phase B ($Mg_{10}Si_3O_{14}F_4$): implications for the role of fluorine in the mantle. *Am. Mineral.* **82**, 647–650.

Kargin A. V., Sazonova L. V., Nosova A. A., Lebedeva N. M., Kostitsyn Y. A., Kovalchuk E. V., Tretyachenko V. V. and Tikhomirova Y. S. (2019) Phlogopite in mantle xenoliths and kimberlite from the Grib pipe, Arkhangelsk province, Russia: Evidence for multi-stage mantle metasomatism and origin of phlogopite in kimberlite. *Geosci. Front.* **10**, 1941–1959.

Keller H., Schwerdtfeger K. and Hennesen K. (1979) Tracer diffusivity of Ca<super>45</super> and electrical conductivity in CaO-SiO_2 melts. *Metall. Trans. B* **10**, 67–70.

Krasnova N. I. (2001) The Kovdor phlogopite deposit, Kola Peninsula, Russia. *Can. Mineral.* **39**, 33–44.

Lee M. J., Garcia D., Moutte J. and Lee J. I. (2003) Phlogopite and tetraferriphlogopite from phoscorite and carbonatite associations in the Sokli massif, Northern Finland. *Geosci. J.* **7**, 9–20.

Li H. and Hermann J. (2017) The effect of fluorine and chlorine on trace element partitioning between apatite and sediment melt at subduction zone conditions. *Chem. Geol.* **473**, 55–73.

Li Y., Jiang H. and Yang X. (2017) Fluorine follows water: Effect on electrical conductivity of silicate minerals by experimental constraints from phlogopite. *Geochim. Cosmochim. Acta* **217**, 16–27.

Li Y., Yang X., Yu J. H. and Cai Y. F. (2016) Unusually high electrical conductivity of phlogopite: the possible role of fluorine and geophysical implications. *Contrib. Mineral. Petrol.* **171**, 37, doi: 10.1007/s00410-016-1252–x.

Liu D., Smyth J. R., Zhu X., Miao Y., Hu Y., Chen G. and Ye Y. (2021) High-pressure vibrational spectra of humite-group minerals: Fluorine effect on thermodynamic properties and hydrogen bonds. *Phys. Earth Planet. Inter.* **312**, 106654.

Liu H., Zhu Q. and Yang X. (2019) Electrical conductivity of OH-bearing omphacite and garnet in eclogite: the quantitative dependence on water content. *Contrib. Mineral. Petrol.* **174**, 57, doi: 10.1007/s00410-019-1593-3

Liu H., Zhang K., Ingrin J. and Yang X. (2021a) Electrical conductivity of omphacite and garnet indicates limited deep water recycling by crust subduction. *Earth Planet. Sci. Lett.* **559**, 116784, doi: 10.1016/j.epsl.2021.116784.

Liu H., Zhu Q., Xu X., Fei H. and Yang X. (2021b) High electrical conductivity of olivine at oxidizing conditions of the shallow mantle and geophysical implications. *J. Geophys. Res. Solid Earth* **126**, e2021JB022739, doi: 10.1029/2021JB022739.

Liu H., Zhu Q. and Yang X. (2019) Electrical conductivity of fluorite and fluorine conduction. *Minerals* **9**, 72, 10.3390/min9020072.

Marcolongo A. and Marzari N. (2017) Ionic correlations and failure of Nernst-Einstein relation in solid-state electrolytes. *Phys. Rev. Mater.* **1**, 025402.

Matano C. (1933) On the relation between the diffusion-coefficients and concentrations of solid metals. *Jpn. J. Phys.* **8**, 109–113.

Müller T., Dohmen R., Becker H. W., Ter Heege J. H. and Chakraborty S. (2013) Fe–Mg interdiffusion rates in clinopyroxene: experimental data and implications for Fe–Mg exchange geothermometers. *Contrib. Mineral. Petrol.* **166**, 1563–1576.

Mysen B. O. and Boettcher A. L. (1975) Melting of a hydrous mantle: I. phase relations of natural peridotite at high pressures and temperatures with controlled activities of water, carbon dioxide, and hydrogen. *J. Petrol.* **16**, 520–548.

Newsom H. E. (1995) Composition of the solar system, planets, meteorites and major terrestrial reservoirs. In *Global Earth Physics: A Handbok of Physical Constants* (ed. T. J. Ahrens). American Geophyscial Union, Washington. pp. 159–189.

Poe B. T., Romano C., Nestola F. and Smyth J. R. (2010) Electrical conductivity anisotropy of dry and hydrous olivine at 8 GPa. *Phys. Earth Planet. Inter.* **181**, 103–111.

Rimsaite J. (1970) Anionic and cationic variations in zoned phlogopite. *Contrib. Mineral. Petrol.* **29**, 186–194.

Roberge M., Bureau H., Bolfan-Casanova N., Frost D. J., Raepsaet C., Surble S., Khodja H., Auzende A. L. and Fiquet G. (2015) Is the transition zone a deep reservoir for fluorine? *Earth Planet. Sci. Lett.* **429**, 25–32.

Robert J., Beny J., Della Ventura G. and Hardy M. (1993) Fluorine in micas: crystal-chemical control of the OH-F distribution between trioctahedral and diocthedral sites. *Eur. J. Mineral.* **5**, 7–18.

Rouxhet P. G. (1970) Hydroxyl stretching bands in micas: a quantitative interpretation. *Clay Miner.* **8**, 375–388.

Sallet R., Price J. D. and Moritz R. (2018) Natural and experimental fluorine substitution in biotite: Implications for fluid-rock thermochronometry and application to the Seridó Belt, northeastern Brazil. *Chem. Geol.* **482**, 32–45.

Schmidt M. W. and Poli S. (2014) Devolatilization During Subduction. In *Treatise on Geochemistry* The Crust (Vol. 4). Elsevier. pp. 669–701.

Shuai K. and Yang X. (2017) Quantitative analysis of H-species in anisotropic minerals by polarized infrared spectroscopy along three orthogonal directions. *Contrib. Mineral. Petrol.* **172**, 14, doi: 10.1007/s00410-017-1336–2.

Smith J. V. (1981) Halogen and phosphorus storage in the Earth. *Nature* **289**, 762–765.

Stormer J. C. and Carmichael I. S. E. (1971) Fluorine-hydroxyl exchange in apatite and biotite: A potential igneous geothermometer. *Contrib. Mineral. Petrol.* **31**, 121–131.

Su W., Baker D. R., Pu L., Bai L., Liu X. and O'Shaughnessy C. (2015) Chlorine-hydroxyl diffusion in pargasitic amphibole. *Am. Mineral.* **100**, 138–147.

Sudo A. and Tatsumi Y. (1990) Phlogopite and K-amphibole in the upper mantle: implication for magma genesis in subduction zone. *Geophys. Res. Lett.* **17**, 29–32.

Symonds R. B., Rose W. I., Bluth G. J. S. and Gerlach T. M. (1994) Volcanic gas studies: methods, results and applications. *Rev. Mineral.* **30**, 1–66.

Yang X. (2012) Orientation-related electrical conductivity of hydrous olivine, clinopyroxene and plagioclase and implications for the structure of the lower continental crust and uppermost mantle. *Earth Planet. Sci. Lett.* **317–318**, 241–250.

Yang X., Keppler H., McCammon C. and Ni H. (2012) Electrical conductivity of orthopyroxene

and plagioclase in the lower crust. *Contrib. Mineral. Petrol.* **163**, 33–48.

Yang X., Keppler H., McCammon C., Ni H., Xia Q. and Fan Q. (2011) The effect of water on the electrical conductivity of lower crustal clinopyroxene. *J. Geophys. Res.* **116**, B04208, doi: 10.1029/2010JB008010.

Yang X. and McCammon C. (2012) Fe^{3+}-rich augite and high electrical conductivity in the deep lithosphere. *Geology* **40**, 131–134.

Zhang B., Li B., Zhao C. and Yang X. (2019) Large effect of water on Fe–Mg interdiffusion in garnet. *Earth Planet. Sci. Lett.* **505**, 20–29.

Figure captions

Fig. 1 Sketch of the pseudo-hexagonal shape of phlogopite and images of the starting samples.

Fig. 2 Capsule design of diffusion experiments.

Fig. 3 (a) BSE image of a recovered sample (1 GPa, 800 °C, ⊥(110) and 240 hours), and (b) BSE image of magnified zone in (a) and elemental mapping of fluorine. Fractures in (a) were caused in the final sample decompression. Crystal-crystal interface of the diffusion couples is marked by arrows and dashed line.

Fig. 4 Example composition profiles of (a) fluorine, (b) potassium and (c) titanium. Observed crystal-crystal interface and modelled Matano interface are shown. Fit curves of fluorine profile in (a) by Eq. (1a) and (1b) coincide with each other.

Fig. 5 Experimentally measured diffusion coefficients of fluorine. Solid lines are fits to data along different directions (r^2 values of fittings are shown).

Fig. 6 (a) diffusion of species in phlogopite, and (b) diffusion of fluorine in silicates. Data sources: (a) Ar (E60), Ar (G74) and Ar (G77) are Ar chemical diffusion in vacuum (Evernden et al., 1960), at 0.2 GPa (Giletti, 1974) and at 1.5 GPa (Giletti and Tullis, 1977), respectively, O (F91, ⊥*c*) and O (F91, //*c*) are O self diffusion (⊥*c* and //*c*) at 0.1 GPa (Fortier and Giletti, 1991), and Sr (H00, //*c*) is Sr chemical diffusion (//*c*) at 1 bar (Hammouda and Cherniak, 2000); and (b) biotite (S18, ⊥*c*) is F chemical diffusion ⊥*c* at 0.4 GPa (Sallet et al., 2018) and titanite (B08) is F chemical diffusion at 0.5-1 bars (Berds et al., 2008). Direction //*c* in available reports corresponds to ⊥(001) in this study.

Fig. 7 A comparison of theoretically calculated and laboratory measured

conductivity of phlogopite with 2.75 wt.% fluorine. Measured data are from Li et al. (2016), and calculated data are by Eq. (5) and diffusion parameters in Table 2.

Fig. 8 Closure temperature of fluorine in phlogopite. (a) closure temperature by Eq. (6a), with assumed cooling rates of 100 (solid lines) and 1 (dashed lines) °C/Myr. S18 is the estimation for fluorine in biotite (⊥c) with the data reported by Sallet et al.(2018). (b) closure temperature by Eq. (6b) with an assumed cooling rate 1 °C/Myr, in which the dependence of T_c on T_0 is accounted (see text). GM is the geometric mean by Eq. (4), and is the same in (a) and (b).

Table 1 Chemical composition of starting and recovered samples (wt. %)

	SiO_2	TiO_2	Al_2O_3	FeO	MgO	Na_2O	K_2O	F	O = F	Total	H_2O
Starting samples											
Phl-A	41.90	0.78	16.72	0.48	26.36	0.94	9.37	0.56	-0.24	96.87	1.23
	0.14	*0.01*	*0.07*	*0.01*	*0.12*	*0.04*	*0.15*	*0.01*			
Phl-B	41.65	0.23	17.44	0.18	27.18	0.08	10.65	2.71	-1.14	98.98	1.04
	0.14	*0.02*	*0.08*	*0.01*	*0.09*	*0.01*	*0.13*	*0.01*			
Recovered samples (Phl-A)											
A210	42.31	0.81	16.70	0.49	26.57	0.93	9.38	0.54	-0.23	97.50	
	0.31	*0.04*	*0.32*	*0.06*	*0.22*	*0.02*	*0.11*	*0.02*			
A217	42.34	0.77	16.74	0.46	26.78	0.93	9.32	0.56	-0.24	97.68	
	0.10	*0.01*	*0.08*	*0.03*	*0.01*	*0.02*	*0.03*	*0.04*			
A216	42.73	0.77	16.40	0.49	26.70	1.15	9.18	0.60	-0.26	97.76	
	0.19	*0.03*	*0.16*	*0.01*	*0.05*	*0.01*	*0.02*	*0.01*			
B377	42.16	0.74	16.38	0.49	26.53	1.00	9.29	0.54	-0.23	96.90	
	0.10	*0.03*	*0.06*	*0.05*	*0.03*	*0.01*	*0.03*	*0.04*			
A230	42.12	0.70	16.98	0.50	26.52	0.93	9.42	0.54	-0.23	97.48	
	0.22	*0.06*	*0.17*	*0.02*	*0.06*	*0.04*	*0.03*	*0.01*			
B331	42.06	0.75	16.42	0.45	26.62	1.04	9.37	0.60	-0.28	97.02	
	0.24	*0.03*	*0.07*	*0.02*	*0.02*	*0.03*	*0.07*	*0.05*			
B327	42.54	0.74	16.25	0.45	26.76	1.01	9.33	0.56	-0.24	97.39	
	0.09	*0.02*	*0.01*	*0.04*	*0.08*	*0.05*	*0.14*	*0.02*			
B332	42.58	0.83	16.56	0.45	26.84	1.00	9.24	0.56	-0.24	97.81	
	0.04	*0.02*	*0.18*	*0.01*	*0.05*	*0.05*	*0.03*	*0.01*			
A227	42.24	0.77	16.48	0.54	26.99	1.00	9.30	0.56	-0.24	97.63	
	0.31	*0.01*	*0.01*	*0.01*	*0.15*	*0.03*	*0.02*	*0.01*			
B324	42.15	0.77	16.67	0.49	26.45	0.94	9.20	0.53	-0.23	96.97	
	0.06	*0.05*	*0.20*	*0.03*	*0.19*	*0.01*	*0.02*	*0.02*			
Recovered samples (Phl-B)											
A210	41.70	0.34	17.23	0.15	27.32	0.09	10.88	2.74	-1.15	99.29	
	0.32	*0.07*	*0.09*	*0.01*	*0.24*	*0.03*	*0.05*	*0.05*			
A217	42.20	0.28	17.07	0.15	27.44	0.06	10.86	2.78	-1.17	99.67	
	0.10	*0.02*	*0.01*	*0.02*	*0.14*	*0.02*	*0.05*	*0.05*			
A216	41.89	0.31	17.07	0.14	27.31	0.08	10.78	2.75	-1.16	99.17	
	0.08	*0.02*	*0.06*	*0.01*	*0.05*	*0.02*	*0.01*	*0.03*			
B377	41.52	0.34	17.16	0.15	27.17	0.07	10.82	2.72	-1.15	98.80	
	0.16	*0.03*	*0.06*	*0.03*	*0.18*	*0.01*	*0.09*	*0.02*			
A230	41.45	0.37	17.18	0.19	27.17	0.09	10.80	2.76	-1.16	98.84	
	0.02	*0.01*	*0.06*	*0.01*	*0.06*	*0.01*	*0.16*	*0.02*			
B331	41.35	0.27	17.05	0.16	27.02	0.11	10.86	2.68	-1.13	98.37	
	0.02	*0.01*	*0.09*	*0.01*	*0.06*	*0.01*	*0.03*	*0.01*			
B327	42.19	0.30	17.22	0.14	27.34	0.06	10.96	2.80	-1.18	99.84	
	0.14	*0.01*	*0.06*	*0.04*	*0.25*	*0.01*	*0.02*	*0.01*			

B332	41.96	0.27	17.05	0.09	27.20	0.09	10.90	2.72	-1.15	99.12
	0.14	*0.04*	*0.04*	*0.01*	*0.28*	*0.01*	*0.01*	*0.11*		
A227	41.90	0.28	17.11	0.18	27.18	0.10	10.80	2.69	-1.13	99.11
	0.05	*0.01*	*0.23*	*0.01*	*0.01*	*0.01*	*0.09*	*0.03*		
B324	41.88	0.35	17.17	0.14	27.43	0.07	10.80	2.76	-1.16	99.44
	0.14	*0.05*	*0.15*	*0.01*	*0.14*	*0.01*	*0.13*	*0.02*		

Data are the average of multi-point analyses (all Fe as FeO), and data in the italic are the standard deviation. Fluorine contents in rims close to diffusion interface were not included. Mn, Cr, Ca and Ni contents are usually ~0.01 wt.%, and are not shown (note: natural phlogopites contain large amounts of BaO, ranging from <1 wt.% to ~10 wt.%). Water contents are given as the equivalent amount of H_2O, and uncertainty is about 10-15% (see text).

Table 2 Summary of experimental conditions and fit parameters

	P (GPa)	T (°C)	Direction	Duration (h)	log D (m^2/s)*	log D (m^2/s)#	log D_0 (m^2/s)	E (kJ/mol)
A210	1	700	⊥(001)	240	-19.14 ± 0.03	-19.15 ± 0.48		
A217	1	750	⊥(001)	200	-18.58 ± 0.12	-18.55 ± 0.17	-5.94 ± 0.87	246 ± 16
A216	1	800	⊥(001)	25	-17.83 ± 0.13	-17.86 ± 0.45		
B377	1	800	⊥(001)	150	-17.93 ± 0.10	-17.88 ± 0.11		
A230	1	700	⊥(010)	255	-18.46 ± 0.14	-18.52 ± 0.20		
B331	1	750	⊥(010)	250	-17.99 ± 0.15	-17.98 ± 0.22	-7.87 ± 0.58	198 ± 11
B327	1	800	⊥(010)	260	-17.47 ± 0.15	-17.45 ± 0.21		
B332	1	700	⊥(110)	226	-18.20 ± 0.12	-18.20 ± 0.20		
A227	1	750	⊥(110)	264	-17.72 ± 0.08	-17.68 ± 0.15	-8.75 ± 0.22	176 ± 4
B324	1	800	⊥(110)	240	-17.32 ± 0.07	-17.31 ± 0.10		
GM							-7.42 ± 0.61	205 ± 10

*, diffusion coefficient calculated by Eq. (1a).

#, diffusion coefficient calculated by Eq. (1b).

Fit parameters (D_0 and E) are obtained by Eq. (2), and GM are the geometric mean by applying Eq. (4).

Declaration of interests

☒ The authors declare that they have no known competing financial interests or personal relationships that could have appeared to influence the work reported in this paper.

☐The authors declare the following financial interests/personal relationships which may be considered as potential competing interests:

Figure 1

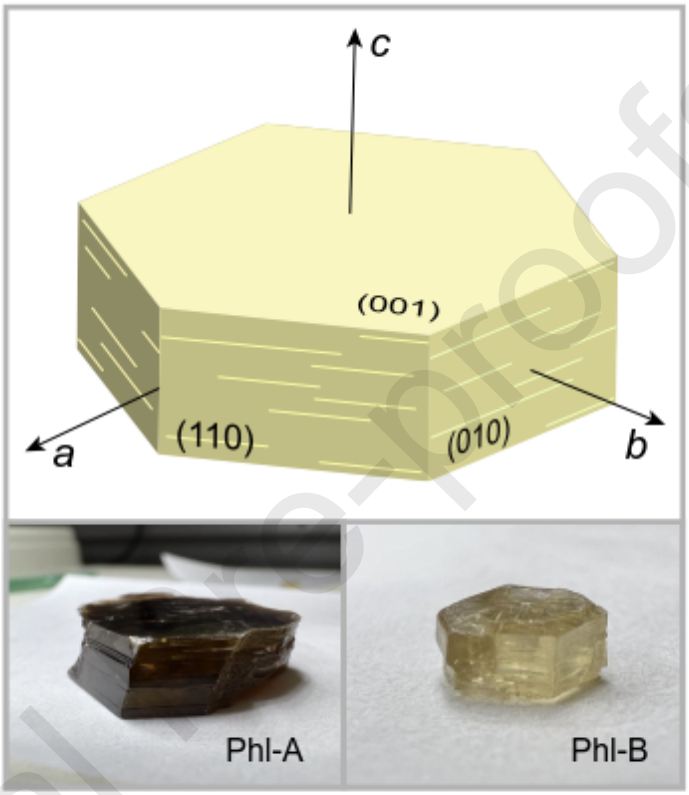

Figure 2

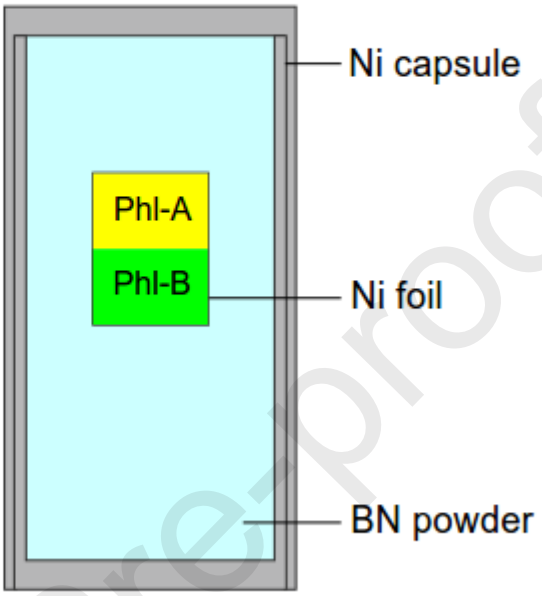

Figure 3

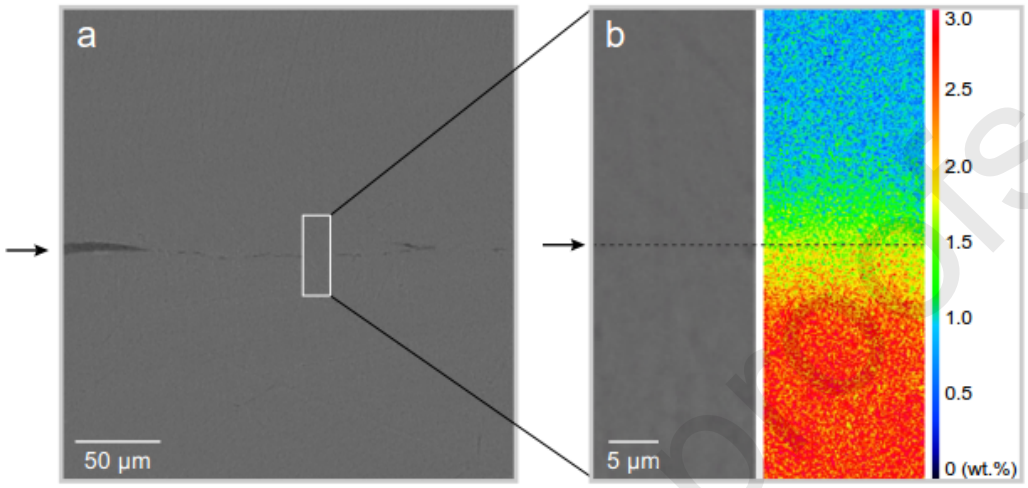

Figure 4

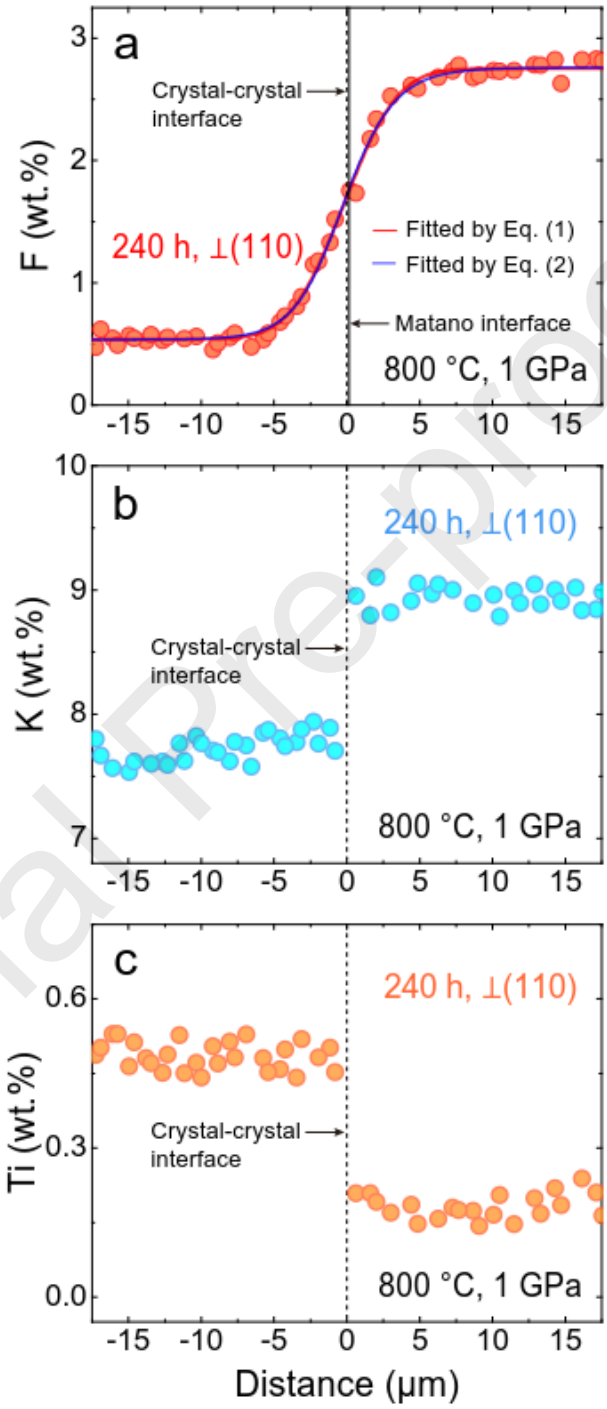

Figure 5

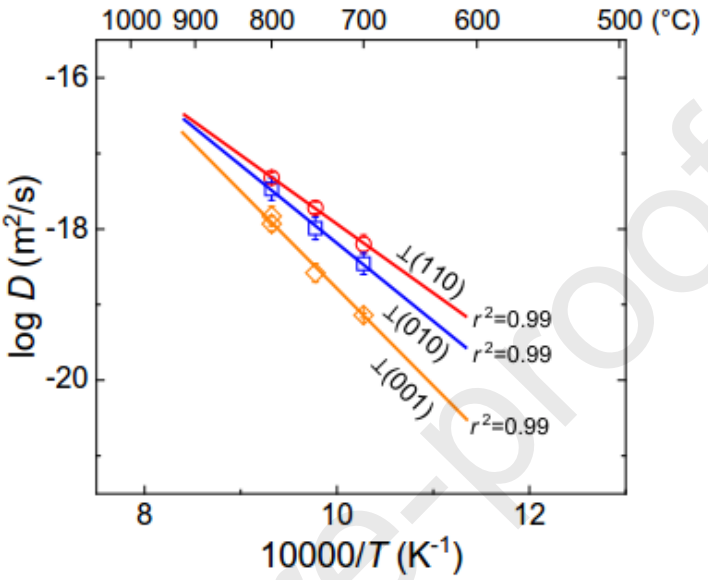

Figure 6

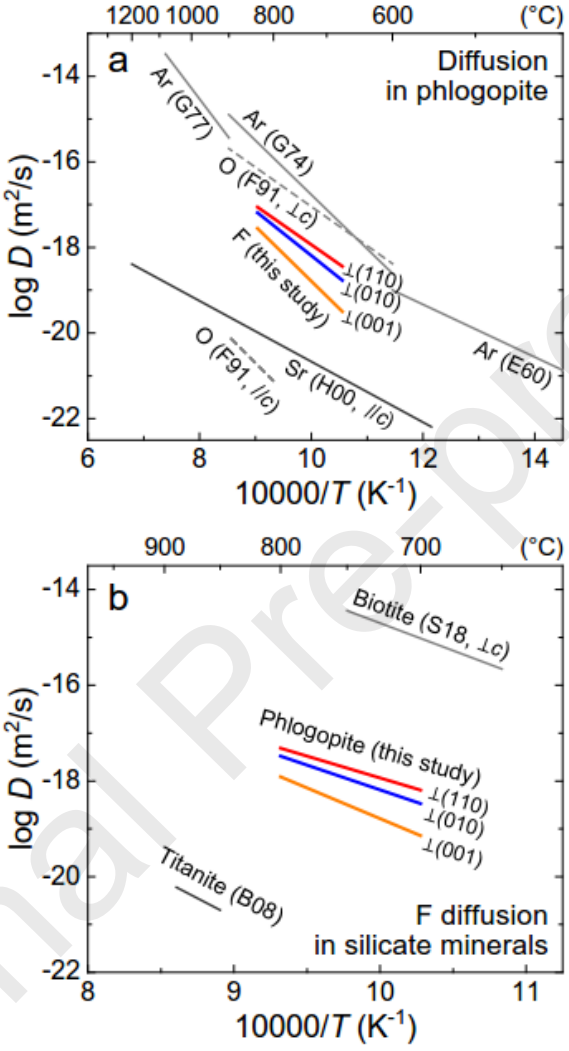

Figure 7

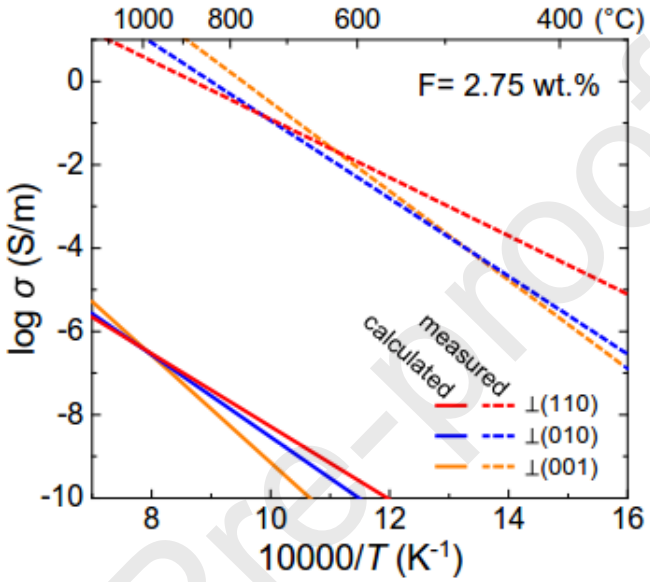

Figure 8